Optica Applicata, Vol. LV, No. 3, 2025
DOI: 10.37190/oa/205978

Research on optical fiber sensing strain field prediction algorithm based on machine learning

Juan Li[1], Lili Zhao[1,*], Ziyi Yin[2]

[1] College of Information Engineering, Changchun College of Electronic Technology, Jilin Changchun, 13000, China

[2] School of Information Science and Technology, Northeast Normal University, Jilin Changchun, 13000, China

To accurately predict the strain field distribution at the assembly position and achieve online calibration of the assembly process, built on an online monitoring system for assembly status based on FBGs network. The installation positions of various FBG sensors were designed through strain field simulation analysis. A strain field prediction model based on support vector machine (SVM) algorithm was designed. It uses FBGs data to predict the strain field distribution at the assembly position for correcting the assembly position and posture. In the calibration experiment, the strain response curves of six FBG sensors were tested, and their linearity was above 0.98. The maximum sensitivity was 2.67 pm/N and the minimum sensitivity was 1.12 pm/N. Three typical assembly anomalies were compared. For different types of assembly anomalies, the response wavelength values and distribution characteristics of each FBG sensor have significant differences. For the same type of assembly anomaly, there is a good linear relationship between the response wavelength values and strain values. In the prediction experiment, the maximum error of strain prediction for the validation set was 4.37 με, and the average error was 2.54 με. The predicted results are close to the training set results.

Keywords: fiber optic sensing, strain field prediction, machine learning, support vector machine (SVM) algorithm.

1. Introduction

The global manufacturing industry is moving from automation to intelligence [1]. In traditional manufacturing, automatic control can complete the assembly task of products. But the product structure becomes increasingly complex, and the assembly process is no longer simply repetitive work [2]. The prerequisite for achieving intelligent assembly control is to accurately and comprehensively obtain the strain field distribution in the assembly area, so strain field prediction technology has become a new research hotspot.

The Boeing Company was the first to introduce the iGPS 3D measurement system in aircraft docking operations, which played an important role in precision docking of

large structures [3,4]. The accuracy of iGPS is generally around 0.1 mm, and its testing accuracy is high. The advantage of optical scanning is non-contact and high accuracy, but it cannot obtain strain field distribution. MARGUET *et al*. [5] studied measurement assisted assembly (MAA) applicable to the overall assembly of passenger aircraft, which can calibrate the assembly process by obtaining strain and temperature data. VICHARE *et al*. [6] analyzed the strain data of the assembly and derived the deformation of the assembly under strain. Electric strain sensors can obtain strain information, but they are susceptible to electromagnetic interference and pose a risk of electrostatic damage when installed on metal robotic arms. This method requires high openness in the assembly environment, but the actual working environment often does not have it. Secondly, external interference such as vibration during the assembly process significantly interferes with laser measurement. The use of fiber optic sensing can avoid the problem of environmental openness, and at the same time, environmental vibration interference can be eliminated through differential processing of multiple FBG signals.

Compared to other methods, fiber optic sensing technology is not affected by electromagnetic interference, and its small size can be installed in almost any assembly position. Because it is passive, it has advantages such as moisture resistance and corrosion resistance. NICOLAS *et al*. [7] installed a large number of FBG sensors on aircraft wings to obtain strain field information of the wings. YI *et al*. [8] has developed a multi-fingers robotic arm. It can control the magnitude of applied force based on FBGs, with a strain control accuracy of 6.0 N. WANG *et al*. [9] achieved linear feedback control in the range of 0.2–3.4 N using FBG sensors network. HOU *et al*. [10] designed a grasping structure through fiber optic sensing, with a feedback speed of only 0.8 s. LIU *et al*. [11-13] proposed a strain distribution detection method for free-form surfaces based on FBG arrays, and tested the strain distribution trends of free-form surfaces under five different strain conditions. They achieved flexible assembly and docking of earpiece structures through fiber optic sensing networks, with strain sensitivity better than 24.5 pm/N. YU *et al*. [14] proposed an intelligent detection and correction system based on fiber optic sensing network to achieve adaptive control of product installation. The experiment showed that the relative error of the inversion accuracy of its position was better than 10.0%. Fiber optic sensing networks can obtain strain information from the testing location and fuse this information to form a strain field prediction model, in order to complete feedback control for intelligent assembly. This article uses the support vector machine (SVM) algorithm in mechanical learning technology to predict the changes in the strain field during the assembly process, providing quantitative guidance for the assembly process.

2. System composition and working principle

The system includes a fiber optic sensing network, a data acquisition module, and a data processing module. It controls the mechanical gripper to complete the operation process of assembling the assembly to the assembly position, as shown in Fig. 1.

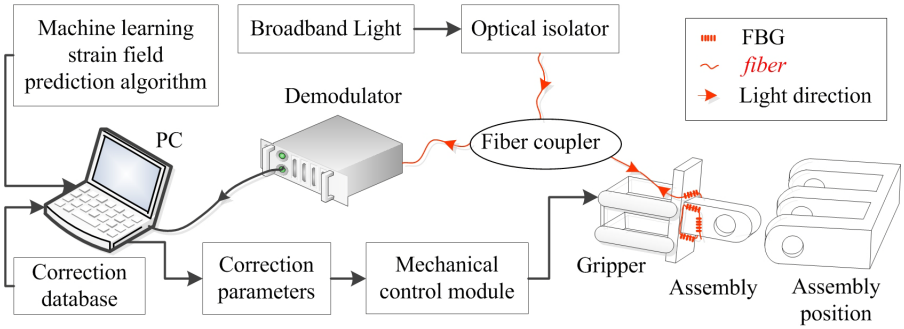

Fig. 1. Assembly calibration system based on fiber optic strain field prediction algorithm.

The broadband light source emits broadband light, which enters the fiber coupler after passing through the optical isolator. The fiber coupler adopts a 1-2 structure design. Broadband light enters the FBG sensing network on the assembly. It collects wavelength changes at corresponding positions, and then the test data is returned to the demodulator by the fiber coupler. The computer analyzes the test strain field based on machine learning strain field prediction algorithms and preset standard data. It predicts its changing trend and completes online correction. The correction constant adjusts the pose of the assembly by manipulating the mechanical gripper through the mechanical control module. Finally, the assembly error was corrected. As shown in Fig. 1, the assembly on the left side is movable. The assembly position on the right is fixed.

3. Strain field simulation and FBG layout design

The material used for simulating the assembly structure is structural steel, with a Poisson's ratio of 0.3 and a Young's modulus of 2×10^{11} Pa. The dimensions of the bottom structure are 200 mm × 100 mm × 10 mm. The angle of the assembly ear hole is 75°, the height is 89.09 mm, and the thickness is 10 mm. The diameter of the central ear hole is 25 mm, and the diameter of the four small ear holes around it is 6 mm. The stress position is 100 N, and three positions are tested separately.

The placement of FBG on the assembly is very important. FBG sensors can obtain continuous strain information at the assembly position, thereby providing real-time feedback on the assembly status. It can correct assembly errors and achieve online calibration of the assembly process. In order to lay the FBG sensor at the most sensitive position of the assembly structure, external strain simulation analysis was conducted on the assembly structure in ANSYS, as shown in Fig. 2(a)–(c).

When there is a displacement error in the vertical direction (referred to as situation A), additional strain will be generated at the compression position. When the external strain is set to 100 N in the simulation, the strain field distribution is shown in Fig. 2(a), with the most sensitive position in the red area and the maximum deformation

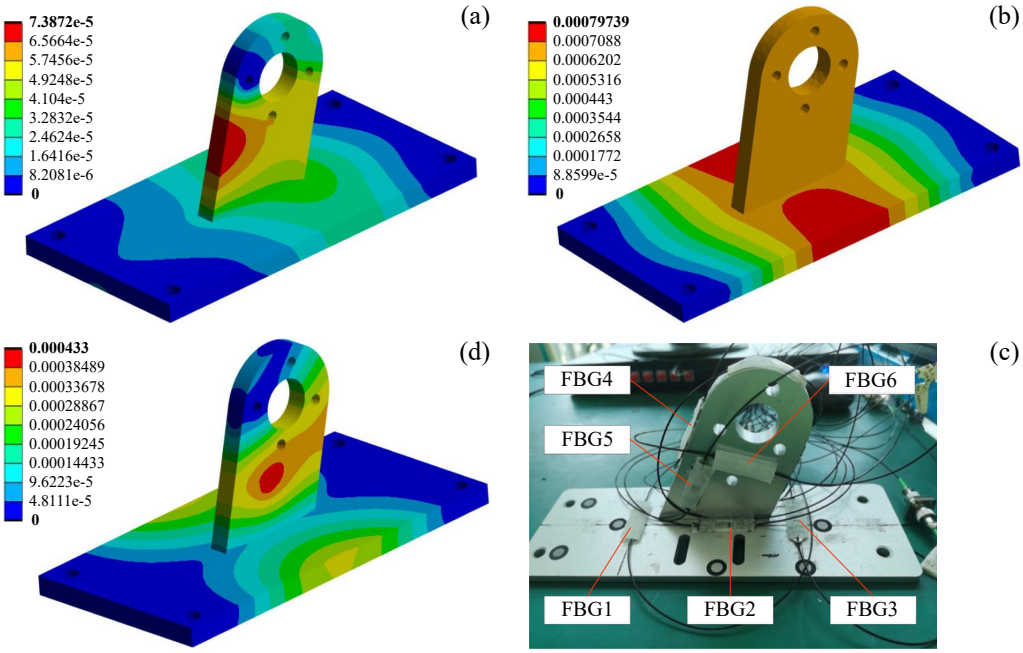

Fig. 2. Strain field distributions corresponding to different assembly abnormal states. (a) Vertical displacement error. (b) Insertion direction displacement error. (c) Position error. (d) Distribution of FBG on the physical assembly.

of 7.3872×10^{-5} mm. The distribution of stress field gradually decreases along the ear hole direction from the maximum position, and stress attenuation is significant in the bottom structure. When there is a displacement error in the insertion direction (referred to as situation B), the strain field distribution is shown in Fig. 2(b), with the most sensitive position in the red area and the maximum deformation of 7.9739×10^{-4} mm. The stress field is strongest on both sides of the bottom center position and gradually decreases as it extends towards both ends. The stress values in the ear canal are similar. When there is an error in the assembly posture (referred to as situation C), the strain field distribution is shown in Fig. 2(c), with the most sensitive position in the red area and the maximum deformation of 4.33×10^{-4} mm. The distribution of stress field spreads out from the position of the stress point, and the stress is more concentrated in the direction biased towards the ear hole. The stress values on the bottom surface increase on both sides of the center position, which is opposite to the stress field distribution characteristics of situation A. From Fig. 2(a)–(c), the abnormal form of strain field varies for different assembly errors. It proves the feasibility of quantifying assembly anomalies and guiding assembly correction using FBG sensing network test data. Based on the simulation results of different positions, six FBG sensors were installed at several sensitive locations of the assembly, as shown in Fig. 2(d). In the test,

image recognition is used to perform real value testing on the position of the test structure, in order to calculate the error of the inverted position of the fiber optic sensor.

4. Strain field prediction model by SVM

Firstly, the strain loading device is used to apply external strain to the assembly in the process of predicting assembly strain. Each FBG sensor collects the wavelength response at the corresponding position and inverts it into strain data. Then, we construct a solution model suitable for assembly error correction in the SVM model, and train the model to analyze the trend of strain field changes based on test data from FBG sensors. It calculates its deviation from the standard position to complete the correction of assembly position and posture. The test data of FBG sensors is used as the input/output set, and a nonlinear mapping relationship is set between load requirements and strain data. If some of the test data is used as input and the other part is used as output, the functional relationship is as follows:

$$f\colon \varepsilon_a \to \varepsilon_d \tag{1}$$

Then it is transformed into the optimal problem corresponding to the variable input value ε_i, and its support vector machine model [15] is

$$\min \frac{1}{2}\omega^{\mathrm{T}}\omega + c\sum_{i=1}^{n}\mu_i\xi_i \qquad \text{s.t.}\begin{cases}\varepsilon_{d_i}(\omega\varepsilon_{\mathrm{i}} + d) \geq 1 - \xi_i \\ \xi_i \geq 0\end{cases} \tag{2}$$

Among them, ω is the slope of the optimal hyperplane in the support to the vector machine, c is the penalty coefficient, n is the number of test points, μ_i is the weight coefficient, ξ_i is the relaxation variable, and d is the intercept of the optimal hyperplane. Simplifying Eq. (2), there are

$$\min_{\alpha} \frac{1}{2}\alpha^{\mathrm{T}}Q\alpha - e^{\mathrm{T}}\alpha \qquad \text{s.t.}\begin{cases}\varepsilon_d^{\mathrm{T}} \geq 0 \\ 0 \leq \alpha_i \leq \mu_i c_i, \quad i = 1, 2, \ldots, n\end{cases} \tag{3}$$

Among them, α is the Lagrange multiplier, Q is a semi-positive definite matrix of $n \times n$, and $e = [1, 2, ..., n]^{\mathrm{T}}$.

$$Q_{ij} = \begin{bmatrix}\varepsilon_{d_1} \\ \varepsilon_{d_2} \\ M \\ \varepsilon_{d_i}\end{bmatrix}\begin{bmatrix}\varepsilon_{d_1} \\ \varepsilon_{d_2} \\ M \\ \varepsilon_{d_j}\end{bmatrix} K(\varepsilon_{a_i}, \varepsilon_{a_j}), \qquad K(\varepsilon_{a_i}, \varepsilon_{a_j}) = K\left(\begin{bmatrix}\varepsilon_{a_1} \\ \varepsilon_{a_2} \\ M \\ \varepsilon_{a_i}\end{bmatrix}\begin{bmatrix}\varepsilon_{a_1} \\ \varepsilon_{a_2} \\ M \\ \varepsilon_{a_j}\end{bmatrix}\right) \tag{4}$$

Among them, $K(\varepsilon_{a_i}, \varepsilon_{a_j})$ is the kernel function equation. ε_{a_i} and ε_{a_j} respectively represent the strain of the i-th and j-th in the x-axis and y-axis directions on the optimal hyperplane. Since Eq. (4) is dual before and after, the optimal solution of ω needs to satisfy

$$\omega = \sum_{i=1}^{n} \varepsilon_{d_i} \begin{bmatrix} \alpha_1 \\ \alpha_2 \\ M \\ \alpha_i \end{bmatrix} g\left(\begin{bmatrix} \varepsilon_{a_1} \\ \varepsilon_{a_2} \\ M \\ \varepsilon_{a_i} \end{bmatrix} \right) \tag{5}$$

Among them, $g(\varepsilon_{a_i})$ is the nonlinear mapping of ε_{a_i} from the input space R^n to the high -dimensional feature space G; ε_{a_i} represents the strain at the initial state a.

$$R^n \to G: \begin{bmatrix} \varepsilon_{a_1} \\ \varepsilon_{a_2} \\ M \\ \varepsilon_{a_i} \end{bmatrix} \to g\left(\begin{bmatrix} \varepsilon_{a_1} \\ \varepsilon_{a_2} \\ M \\ \varepsilon_{a_i} \end{bmatrix} \right) \tag{6}$$

Finally, the support vector machine model applied for predicting the strain field at the assembly position is

$$\hat{\varepsilon}_d = \mathrm{SGN}\left\{ \sum_{i=1}^{n} \varepsilon_{d_i} \begin{bmatrix} \alpha_1 \\ \alpha_2 \\ M \\ \alpha_i \end{bmatrix} K\left(\begin{bmatrix} \varepsilon_{a_1} \\ \varepsilon_{a_2} \\ M \\ \varepsilon_{a_i} \end{bmatrix}, \begin{bmatrix} \varepsilon_{a_1} \\ \varepsilon_{a_2} \\ M \\ \varepsilon_{a_j} \end{bmatrix} \right) + d \right\} \tag{7}$$

Among them, ε_{a_i} and ε_{a_j} respectively represent the strain of i-th and j-th in the x-axis and y-axis directions on the optimal hyperplane at the initial state a. This nonlinear mapping function can be used for predicting the strain field of assemblies. The strain information of the test is imported into the input end, and the prediction model is started. The output end outputs the predicted strain field result and provides the correction parameters for the calibration fitting error.

5. Experiment

5.1. Calibration and testing of FBG sensors

The laser used in the experimental system is TLS1006F fiber laser, with a wavelength scanning range of 1548 to 1568 nm and a wavelength resolution of 1 pm. The de-

modulation equipment is FI-1511M fiber grating demodulator, with a test band of 1525–1556 nm and a resolution of 1 pm. The assembly control section has 6 degrees of freedom, namely *x*-axis, *y*-axis, and *z*-axis rotation, *xoy* plane rotation, *xoz* plane rotation, and *yoz* plane rotation. The minimum step distance of the robotic arm is 0.5 mm. The minimum control accuracy of the control end is 0.5 mm and 1 deg.

Before assembly testing, all FBG sensors need to be calibrated. The testing range of the strain is 0–200 N, and the center wavelength position of the FBG is tested every 10 N within this range. The results are shown in Fig. 3.

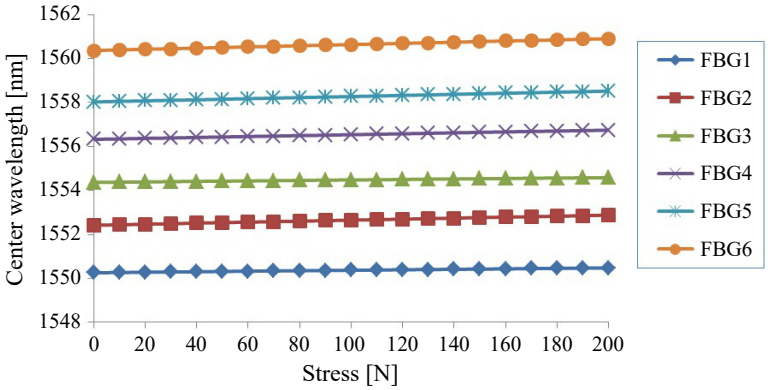

Fig. 3. Strain calibration test curves of 6 FBGs.

From Fig. 3, the strain response curves of the six FBG sensors are all linear, with linearity above 0.98. It proves that when external abnormal strain is applied to the assembly, there is a good linear relationship between the wavelength shift of each FBG and the magnitude of the strain. For different FBG sensors, their strain sensitivity is also different. Although there are the same material and packaging structure for FBG sensors, they are attached to different positions, resulting in varying amounts of wavelength shift. The strain sensitivities of FBG1, FBG2, FBG3, FBG4, FBG5, and FBG6 are 1.12, 2.43, 1.15, 2.26, 2.48, and 2.67 pm/N. Although their materials and packaging are the same, due to the different positions where they are pasted, the degree of deformation they can undergo varies, resulting in significant differences in their response sensitivity. The linearity of the test curves for FBG1, FBG2, FBG3, FBG4, FBG5, and FBG6 are 0.98, 0.98, 0.96, 0.97, 0.96, and 0.97, respectively. There are significant differences in strain response effects at different positions, which indirectly proves that strain field distribution can be used to invert assembly anomaly types and guide correction.

5.2. Pattern analysis for different types of assembly errors

To quantify the effect of assembly errors on various FBG sensors, three common assembly anomalies were measured. The test situation is divided into: in situation A, there is a displacement error in the vertical direction. When the strain is 50 N, it is A1,

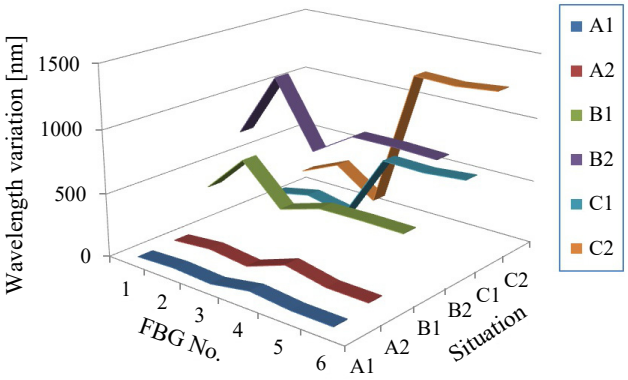

Fig. 4. Wavelength responses of different FBGs under 6 testing conditions.

and when the strain is 100 N, it is A2. In situation B, there is a displacement error in the insertion direction. When the strain is 50 N, it is B1, and when the strain is 100 N, it is B2. In situation C, there is an angle error in the assembly posture. When the strain is 50 N, it is C1, and when the strain is 100 N, it is C2. The deviation strain is set to 50 and 100 N, respectively, in order to compare the influence of strength changes on system identification. The test results are shown in Fig. 4.

Compare the wavelength responses of 6 FBGs under different testing conditions. In situation A1, the wavelength responses of all six FBGs are less than 100 pm. The wavelength response value of FBG4 is the largest, and it is 67.8 pm. When the strain increases from 50 to 100 N (A2), the wavelength response of FBG4 is 137.4 pm. The wavelength increase of other FBGs has also doubled. It proves that the testing process changes linearly. In situation B1, the wavelength response value of FBG2 is the largest, and it is 659.3 pm. When the strain increases from 50 to 100 N (B2), the wavelength response of FBG2 is 1228.4 pm, and it also follows a linear relationship. In situation C1, the wavelength response value of FBG6 is the largest, and it is 643.5 pm. When the strain increases from 50 to 100 N (C2), the wavelength response of FBG6 is 1234.2 pm, and it also follows a linear relationship. Comparing situation A, situation B, and situation C, there are significant differences in the impact of different types of assembly anomalies on FBG wavelength changes. When the same type of anomaly occurs, the effect of different strain intensities on the wavelength variation of FBG has a linear relationship. So using test data from multiple FBGs can not only identify the types of assembly abnormalities, but also quantitatively analyze their status.

5.3. Strain field prediction experiment

On the basis of verifying the response relationship between different types of assembly anomalies and FBG, the predictive performance of the algorithm was tested. Among the 100 sets of data tested, 80 sets were selected as the input set for learning, and 20 sets were used as the validation set. Then they are compared the measurement results with the predicted results and the accuracy of the model prediction is calculated. The ex-

ternal strain on the assembly part is gradually increased in units of 10 N at the assembly position. The loading strains are 10, 20, 30, 40, 50, 60, 70, 80, 90, and 100 N, respectively. Train the prediction training set with 200 sample points and use 40 samples to test the test set. The comparison results between the test set and the prediction set are shown in Fig. 5.

As shown in Fig. 5(a), when the strain value inverted from the test data is the input quantity, the predicted stress value is calibrated near the true value. The error threshold is set to ±2 με, with a mean of 1.57 με. Using the model again for predictive analysis of the validation set, the maximum absolute value of strain prediction error is 4.37 με, the average error is 2.54 με, and the root mean square error is 0.814 με, and the relative errors is 0.981. From the above three indicators to measure accuracy, the machine learning prediction algorithms have high accuracy. As shown in Fig. 5(b), the test data was validated using this algorithm, and the test results were in good agreement with

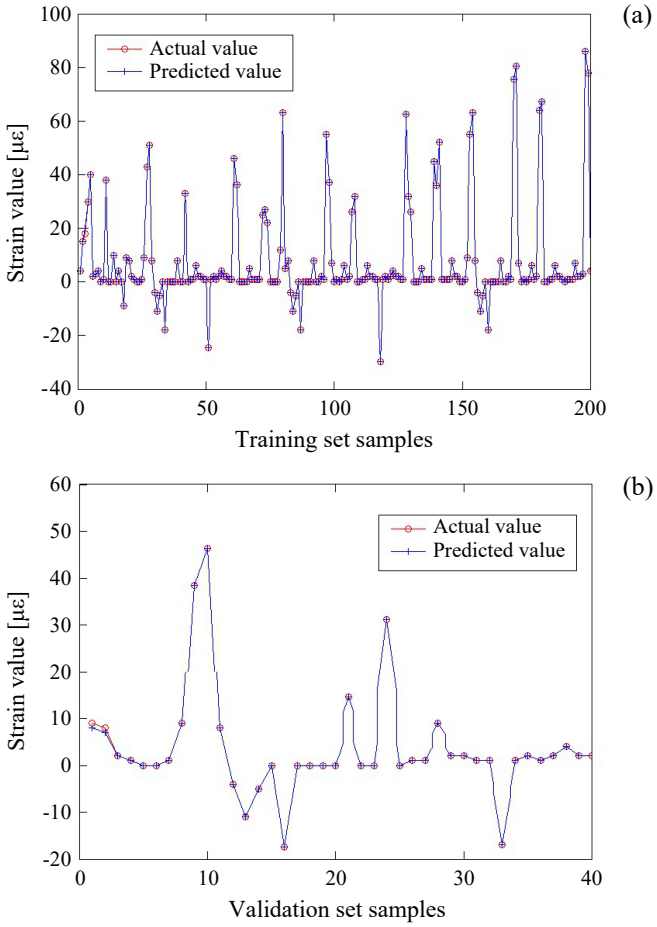

Fig. 5. Comparisons of strain prediction model test results. Prediction results of (a) strain training set, and (b) strain validation set.

the real results, with an average error of less than 1.82 με, indicating that the prediction model can effectively invert the real-time state of the target strain field.

6. Conclusions

Aiming at the intelligent correction problem of assembly abnormalities, an online detection system for assembly strain field based on fiber optic sensing network was built. We designed a strain field prediction model based on machine learning, based on the simulation analysis of the strain field distribution of the assembly structure, and we optimized the distribution design of FBG sensors. For different assembly anomalies, the wavelength response of all FBG sensors was measured in the experiment. The quantitative identification of abnormal states was completed based on their response intensity and distribution trend. The main contribution of the paper is to provide a strain field prediction model. This model can be applied in the field of intelligent assembly, providing quantitative data for identifying and correcting assembly anomalies, and realizing online feedback control based on flexible perception intelligent assembly.

Acknowledgment
This work was supported by Jilin Provincial Natural Science Foundation (20240101226JC); the National Science Foundation of Chinese (61703056).

References

[1] S.I. ELEONSKII, M.D. ZAITSEV, YU.G. MATVIENKO, PISAREV V.S., *Fields of residual stresses near filled assemblage holes of the aircraft wing panel*, Inorganic Materials **60**, 2024: 560-574. https://doi.org/10.1134/S0020168524700626

[2] NAIK V., FAIRCHILD P., TAN X., *Nonlinear compensation of stretchable strain sensors with application to proprioceptive sensing of soft robotic arm*, Smart Materials and Structures **34**(3), 2025: 035018. https://doi.org/10.1088/1361-665X/adb2c7

[3] KANG S., TESAR D., *A noble 6-DOF measurement tool with indoor GPS for metrology and calibration of modular reconfigurable robots*, IEEE ICM International Conference on Mechatronics, 2004.

[4] KHREISHI M., OHL R.G., HOWARD J.M., PAPA J.C., MCCLELLAND R., HOVIS C., HADJIMICHAEL T., THOMPSON P., RANSON K., LIANG R., GORIUS N., *Enabling precision coordinate metrology for universal optical testing and alignment applications*, Optical Engineering **60**(3), 2021: 035106. https://doi.org/10.1117/1.OE.60.3.035106

[5] MARGUET B., RIBERE B., *Measurement-assisted assembly applications on Airbus final assembly lines*, SAE Technical Paper, 2003: 2003-01-2950. https://doi.org/10.4271/2003-01-2950

[6] VICHARE P., MARTIN O., JAMSHIDI J., *Dimensional management for aerospace assemblies: Framework implementation with case-based scenarios for simulation and measurement of in-process assembly variations*, The International Journal of Advanced Manufacturing Technology **70**, 2014: 215-225. https://doi.org/10.1007/s00170-013-5262-9

[7] NICOLAS M.J., SULLIVAN R.W., RICHARDS W.L., *Large scale applications using FBG sensors: Determination of in-flight loads and shape of a composite aircraft wing*, Aerospace **3**(3), 2016: 18. https://doi.org/10.3390/aerospace3030018

[8] YI J., KIM B., CHO K.-J., PARK Y.-L., *Underactuated robotic gripper with fiber-optic force sensing tendons*, IEEE Robotics and Automation Letters **8**(11), 2023: 7607-7614. https://doi.org/10.1109/LRA.2023.3315204

[9] Wang Q., Jia D., Yan B., Teng F., Sun C., Li X., *Rotary robotic gripper with LiDAR-tactile sensor fusion*, Optical Engineering **62**(11), 2023: 114102. https://doi.org/10.1117/1.OE.62.11.114102
[10] Hou Q., Fu Y., Luo M., Lu C., Li G., Sun L., *FBG-based methods for monitoring critical slip point during flexible fingers clamping*, IEEE Sensors Journal **23**(22), 2023: 28067-28074. https://doi.org/10.1109/JSEN.2023.3316280
[11] Liu Z., Hou M., Lin X., Liu T., Guo L., Li L., *Research on strain distribution detection method of freeform surface based on FBG array*, IOP Conference Series: Materials Science and Engineering **490**(6), 2019: 062040. https://doi.org/10.1088/1757-899X/490/6/062040
[12] Liu C., Liu Z., Yin L., *On-line slippage measurement system for optical fiber sensing array*, Infrared and Laser Engineering **51**(3), 2022: 9465-9473 (in Chinese).
[13] Liu Z.C., Yang Z.H., Wang J., Yue L., *Design of modified model of intelligent assembly digital twins based on optical fiber sensor network*, Digital Communications and Networks **10**(5), 2024: 1542-1552. https://doi.org/10.1016/j.dcan.2022.06.013
[14] Yu C.R., Yu A.W., Ma M.Z., Liu Z.C., *Intelligent detection and correction system based on optical fiber sensing network*, Optical Communication Technology, **45**(03), 2021: 28-31 (in Chinese).
[15] Floris I., Adam J.M., Calderón P.A., Sales S., *Fiber optic shape sensors: A comprehensive review*, Optics and Lasers in Engineering **139**, 2021: 106508. https://doi.org/10.1016/j.optlaseng.2020.106508

Received April 21, 2025
in revised form May 21, 2025